





Article

# Enhanced Adsorption of Arsenate from Contaminated Waters by Magnesium-, Zinc- or Calcium-Modified Biochar—Modeling and Mechanisms

Despina Vamvuka \*, Elena Sdoukou, Antonios Stratakis  and Despina Pentari 

School of Mineral Resources Engineering, Technical University of Crete, 73100 Chania, Crete, Greece; esdoukou@tuc.gr (E.S.); astratakis@tuc.gr (A.S.); dpentari@tuc.gr (D.P.)

\* Correspondence: [dvamvouka@tuc.gr](mailto:dvamvouka@tuc.gr)

**Abstract:** The adsorption of arsenate from wastewaters was investigated by applying Mg-, Zn- or Ca-modified nut residue biochar activated by nitrogen/steam. The parameters studied were the contact time, adsorbent dose, initial arsenate concentration and solution pH. The adsorption mechanism was investigated. Various analyses of the material before and after arsenate adsorption were carried out, and experimental data were simulated by applying two isotherm models. The results indicated that the maximum removal efficiency of arsenate was 29.4% at an initial concentration of 10 mg/L. The modification of biochar by Mg, Zn or Ca oxides increased the removal rate significantly, from 49.4% at 100 mg/L As<sup>5+</sup> up to 8%, 97% and 97%, respectively. Zn-modified biochar presented an excellent performance for both low and high As<sup>5+</sup> concentrations. All experimental data were accurately fitted by the Freundlich isotherm model ( $R^2 = 0.94\text{--}0.97$ ), confirming a multilayer adsorption mechanism. For a biochar dose of 2 g/L, the maximum capacity of adsorption was enhanced after Mg-, Zn- or Ca-modification from 12.4 mg/g to 35 mg/g, 50 mg/g and 49 mg/g, respectively. The potential mechanisms of adsorption were ligand exchange, chemical complexation, surface precipitation and electron coordination.

**Keywords:** arsenate; adsorption; wastewaters; modified biochar; steam



**Citation:** Vamvuka, D.; Sdoukou, E.; Stratakis, A.; Pentari, D. Enhanced Adsorption of Arsenate from Contaminated Waters by Magnesium-, Zinc- or Calcium-Modified Biochar—Modeling and Mechanisms. *C* **2024**, *10*, 61. <https://doi.org/10.3390/c10030061>

Academic Editor: Athanasia Tolkou

Received: 4 June 2024

Revised: 5 July 2024

Accepted: 7 July 2024

Published: 10 July 2024



**Copyright:** © 2024 by the authors. Licensee MDPI, Basel, Switzerland. This article is an open access article distributed under the terms and conditions of the Creative Commons Attribution (CC BY) license (<https://creativecommons.org/licenses/by/4.0/>).

## 1. Introduction

Arsenic is a highly toxic and carcinogenic heavy metal to living organisms. It can be naturally derived from lithogenic sources and mobilized by geothermal or biological environments. But most importantly, it can be derived from anthropogenic sources, such as uncontrolled mining activities, the combustion of fossil fuels, petroleum refineries and industries of pesticides, herbicides, fertilizers, crop desiccants and glass manufacturing [1,2]. The most prevalent species are arsenite and arsenate, the latter being less soluble and toxic [3]. The discharge of these species to the soil, surface or groundwater can seriously threaten human health and the whole environment. Thus, the World Health Organization has set the maximum allowable limit in drinking water to 10 µg/L [4,5].

Several technologies have been developed for removing arsenic from contaminated water, including ion-exchange, reverse osmosis, membrane filtration, chemical oxidation, coagulation, precipitation and adsorption [1–3,6–8]. Among these technologies, adsorption is considered more efficient, less costly and easier to operate, with minimum by-products generation [1,2].

Traditionally, active carbon has been used as an efficient adsorbent of heavy metals from wastewaters. However, its high cost arising from the availability and processing of raw materials and disposal and recycling issues [9] limit its large-scale application. On the other hand, biochar, the solid product of the pyrolysis of carbonaceous biomass materials, widely applied as a soil amendment and carbon sink in soils for thousands of years [10], has attracted increased attention recently as an environmentally friendly adsorbent for

organic or inorganic pollutants [1]. Although less efficient than active carbon, biochar can be produced at a low cost from a variety of waste materials [11], it is rich in carbon, it shows great thermal stability and it presents favorable physicochemical properties, such as a large surface area and porosity [3,12,13].

However, biochars possess functional groups that are negatively charged on their surface, limiting the adsorption ability of anionic pollutants such as arsenate, which mainly exists in the environment in the form of the oxyanions  $\text{AsO}_4^{3-}$  or  $\text{AsO}_3^{2-}$  [13]. Several studies reported a low adsorption capacity of agricultural-derived biochars, such as plant residues, empty fruit bunches, rice husks, corn cobs and corn straws for arsenate, ranging between 0.8 mg/g and 7.1 mg/g [7,8,14]. Therefore, the physicochemical properties of biochars should be modified in order to immobilize  $\text{As}^{5+}$  ions from aqueous solutions.

The adsorption of  $\text{As}^{5+}$  ion- on iron oxide-modified biochars has been found to be an effective option for their removal from wastewaters. A  $\text{Fe}_3\text{O}_4$ -loaded activated carbon, using waste biomass, showed an excellent capability for arsenate adsorption, with a maximum capacity of 204.2 mg/g [6]. However, nanosized  $\gamma\text{-Fe}_2\text{O}_3$  particles embedded in cotton wood [10], walnut shell [5] and rice husk [12] biochars exhibited a much lower adsorption capacity of 3.1 mg/g, 1.91 mg/g and up to 0.7 mg/g, respectively. In the case of a MnO-modified corn straw biochar, the maximum adsorption capacity for  $\text{As}^{5+}$  was reported to be 14.4 mg/g [1]; for bismuth impregnated wheat straw biochar, it was 16.2 mg/g [4]; and for KOH-modified corn cobs, it was 31 mg/g [11]. Mg-modified materials for arsenate adsorption have been scarcely used. In one study [13], Mg-Al modified corn stalk was synthesized to immobilize As, Pb and Cd simultaneously. The removal efficiency of arsenate was found to increase from  $-62\%$  to  $52\%$ . Also, there is limited knowledge on the impregnation of ZnO on biochars and its effect on improving solid properties. The results obtained by corn cob-derived ZnO-impregnated biochar showed a maximum equilibrium adsorption capacity of 25.9 mg/g of  $\text{As}^{5+}$  [14]. However, the modification by ZnO has been principally used for organic substances and dyes in photocatalytic experiments and, to a lesser extent, in heavy metals adsorption [15]. Furthermore, to the authors' knowledge, the use of Ca oxides, as impregnation agent for the production of engineered biochar, has been investigated only for rice husks, with a low adsorption capacity of about 0.5 mg/g [12].

Based on the above discussion, the innovation of the present study lies in the investigation of the potential of a nut residue not previously investigated, an almond shell, for the efficient adsorption of  $\text{As}^{5+}$  from contaminated water solutions after its physical activation by nitrogen/steam and its modification by  $\text{MgCl}_2 \cdot 6\text{H}_2\text{O}$ ,  $\text{Zn}(\text{NO}_3)_2 \cdot 4\text{H}_2\text{O}$  and quarry dust, a waste of mortars production as a novel modifier. The objective was to explore the performance of the material by varying experimental parameters, as well as the mechanism of adsorption. Valuable information was provided by carrying out advanced specific analyses of the material before and after  $\text{As}^{5+}$  adsorption and by applying two isotherm models to simulate experimental data.

## 2. Materials and Methods

### 2.1. Raw Material and Pretreatment

The agrowaste used in this work was almond shell (AS), provided by a nuts production industry located in North Greece. The material was ground in a cutting mill, sieved to obtain a particle size less than 500  $\mu\text{m}$  and homogenized by a Jones riffler in order to obtain representative samples for the tests.

Four different feedstocks were prepared for the adsorption experiments: non-modified almond shell biochar (ASB), Mg-modified biochar (ASB-Mg), Zn-modified biochar (ASB-Zn) and Ca-modified biochar (ASB-Ca). For Mg modification, raw AS material was dispersed in  $\text{MgCl}_2 \cdot 6\text{H}_2\text{O}$  solution at a solid-to-liquid ratio of 1/10 and stirred for 24 h at 200 rpm and room temperature. After filtration, the material was dried at  $110^\circ\text{C}$  and then activated as described below. The Mg-modified biochar produced was washed to constant pH with distilled water and dried in the oven at  $110^\circ\text{C}$  before use. For the preparation of Zn-modified feedstock, biochar was mixed with NaOH 0.5 M at a solid-to-liquid ratio of

1:5 and stirred at 200 rpm, while being heated up to 60 °C [14]. Zinc nitrate tetrahydrate  $\text{Zn}(\text{NO}_3)_2 \cdot 4\text{H}_2\text{O}$ , purchased by Sigma-Aldrich Chemical Co. (St. Louis, MO, USA), was then added slowly to the solution, which was heated up to 80 °C and maintained at this temperature for 2 h, to ensure  $\text{Zn}(\text{OH})_2$  and ZnO precipitation. Subsequently, the slurry was introduced in a supersonic bath for about 1 h, filtered, washed with distilled water and dried in the oven overnight at 60 °C. Finally, for the modification of the AS with CaO, the raw material was mixed with quarry dust, a waste of mortars production provided by the Finomix AE company, consisting mainly of calcite and calcite magnesian (Figure 1h [16]), at a mass ratio of 1:1. The mixture was impregnated with distilled water and stirred for 12 h at 120 rpm. The slurry was further stirred at 80 °C for 3 h, filtered, washed with distilled water until neutrality and dried at 110 °C overnight. The modified material was activated by nitrogen/steam, as described below.

## 2.2. Production of the Adsorbent and Characterization

All modified or non-modified materials were physically activated by nitrogen and steam in order to increase their specific surface area and pore volume for the adsorption of  $\text{As}^{5+}$ . The equipment used was a fixed bed reactor unit, presented in detail in a previous investigation [16]. The sample was first pyrolyzed in nitrogen (150 mL/min) up to 700 °C, a temperature which was attained with a furnace heating rate of 10 °C/min and kept for 30 min. Nitrogen gas was then replaced by steam by injecting continuously de-ionized water through a syringe pump, with a flow rate of 0.5 mL/min. A uniform flow of steam was achieved by forcing water through a 2 m tube surrounding the reactor within the furnace before contacting the sample bed. The activation lasted 1 h and was followed by reactor cooling with nitrogen. In the case of quarry dust-modified material, the pyrolysis step was conducted at 750 °C for 2 h to calcine the carbonate of calcium. The content of the quarry dust in CaO was 94.5%, as reported previously by the authors [16].

The biochar was characterized following the European CEN/TC335 standards and employing programmable furnaces and the CHNS ThermoScientific analyzer, model Flash 2000 (Thermo Fisher Scientific Inc., Waltham, MA, USA). The specific surface area and pore volume were measured by the BET method, using the Autosorb 1Q-C-MP equipment of Quantachrome, for relative pressures of 0.015–0.32. Before the test, the sample was out-gassed under vacuum at 200 °C for 1 h. Fourier Transform Infrared Spectroscopy (FTIR) was adopted to identify the chemical functional groups on the biochar's surface before and after arsenate adsorption, using a Spectrum 100 spectrophotometer of Perkin Elmer. FTIR spectra were obtained for the 400–4000  $\text{cm}^{-1}$  range of wave numbers, with a resolution of 4  $\text{cm}^{-1}$ . Finally, any crystalline mineral phases of biochar before and after arsenate adsorption were detected by an X-ray diffractometer (XRD), type S2 Ranger EPS (Bruker AXS, Karlsruhe, Germany). The evaluation of XRD spectra was performed using the COD (Crystallography Open Database) database and DIFFRAC-Plus Evaluation software (v. 12.0., Karlsruhe, Germany).

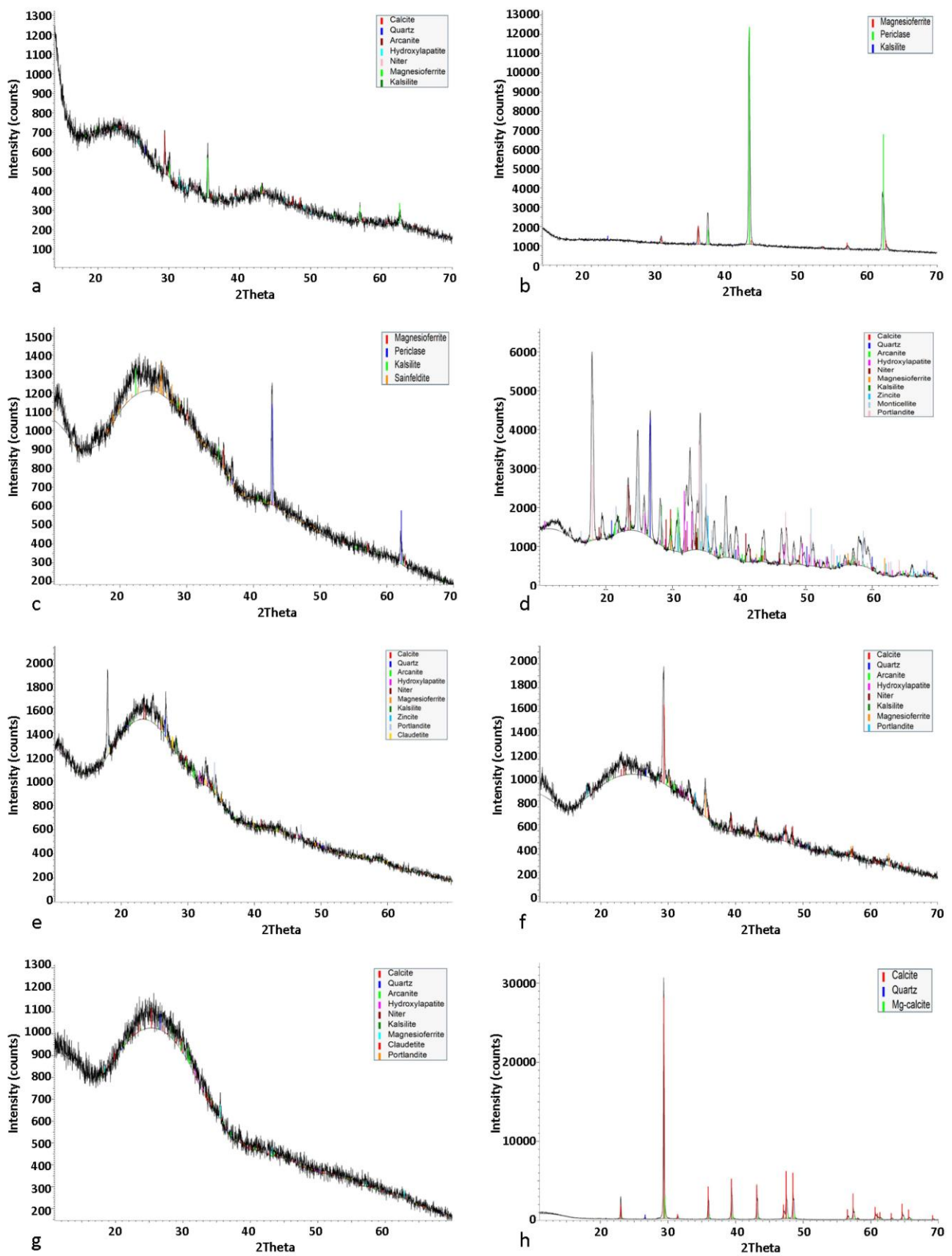


**Figure 1.** XRD spectra of (a) original biochar modified by (b)  $Mg^{2+}$  prior to adsorption, (c)  $Mg^{2+}$  after adsorption, (d)  $Zn^{2+}$  prior to adsorption, (e)  $Zn^{2+}$  after adsorption, (f)  $Ca^{2+}$  prior to adsorption, (g)  $Ca^{2+}$  after adsorption and (h) quarry dust.

### 2.3. Arsenate Adsorption Experiments

The reagent used in the current work was sodium arsenate dibasic heptahydrate ( $\text{Na}_2\text{HAsO}_4 \cdot 7\text{H}_2\text{O}$ ) of analytical grade, purchased by Sigma Aldrich Chemical Co. Arsenate concentrations 5, 10, 25, 50, 75 and 100 mg/L were prepared in de-ionized water. The pH of each solution was adjusted to 6 or 7, using 0.1 M NaOH or 0.1 M HCl.

For the kinetic experiments, the adsorbent was immersed in a 10 mg/L standard arsenate solution at a load of 4 g/L and stirred at 200 rpm on a mechanical shaker for 24 h at room temperature. Liquid samples were withdrawn and filtered after specific contact times up to 24 h. The aliquot pH was measured again and then analyzed by an inductively coupled plasma mass spectrometer ICP-MS, model 7500× of Agilent Technologies (Santa Clara, CA, USA), assisted by an Anton Paar Multiwave 3000 oven (Anton Paar GmbH, Graz, Austria) for the digestion of the samples, to determine the amount of residual  $\text{As}^{5+}$  in each solution. The heavy metal concentration adsorbed by the biochar was calculated as a difference of the initial and final aqueous concentration values.

Once the equilibrium contact time was established, the  $\text{As}^{5+}$  adsorption experiments were carried out following the same experimental conditions as before for all arsenate solution concentrations prepared. Duplicate tests were performed, and the data are reported as average values.

### 2.4. Equilibrium and Adsorption Modelling

The pseudo-first-order model (Equation (1)) and the pseudo-second-order model (Equation (2)) were used to simulate the kinetic tests [4,8]:

$$\log(q_e - q_t) = \log q_e - \frac{k_1}{2.303} t \quad (1)$$

$$\frac{t}{q_t} = \frac{1}{k_2 q_e^2} + \frac{t}{q_e} \quad (2)$$

The modelling of the adsorption data and the determination of the adsorption capability of the biochar under study were performed by adopting the Langmuir (Equation (3)) and Freundlich (Equation (4)) isotherm models [8,11]:

$$\frac{C_e}{q_e} = \frac{1}{bC_e} + \frac{C_e}{Q} \quad (3)$$

$$\log q_e = \log k + \frac{1}{n} \log C_e \quad (4)$$

## 3. Results and Discussion

### 3.1. Properties of Non-Modified and Modified Adsorbent Materials

As Table 1 shows, the biochar of AS generated after nitrogen/steam activation was rich in organic matter and carbon, had a low content of minerals and hydrogen, and was free of nitrogen and sulfur, implying no toxic emissions during processing. However, the oxygen concentration was high, making the material more hydrophilic, with increased polarity [17,18]. The specific surface of the non-modified biochar was enhanced after the nitrogen/steam thermal treatment, and it was about 260 times higher than that of the raw material (2.5 m<sup>2</sup>/g). The microporosity was also increased. The elemental concentration of AS biochar is within the range of values reported for hard wood [18]. The specific surface area and pore volume are higher than most reported data for various biochar materials, ranging between 61 and 349 m<sup>2</sup>/g and 10 and 29 × 10<sup>-2</sup> cm<sup>3</sup>/g, respectively [1,2,4,6,13]. On the other hand, all modified samples presented lower values of the specific surface area (ASB-Mg: 108 m<sup>2</sup>/g, ASB-Zn: 453 m<sup>2</sup>/g, ASB-Ca: 120 m<sup>2</sup>/g), which could be assigned to the coverage of the solid surface by the oxides of MgO, ZnO and CaO, respectively, or the dilution effect.



**Table 1.** Chemical and structural characteristics of biochar (% dry) \*.

Fixed Carbon	Ash	C	H	N	O	S	Specific Surface Area (m <sup>2</sup> /g)	Micropore Volume × 10 <sup>2</sup> (cm <sup>3</sup> /g)	Average Pore Size(Å)
97.5	2.5	66.0	1.1	-	30.4	-	657.0	32.9	24.0

\* "-" not applicable or below detection limits.

The XRD spectra of all adsorbent materials studied before and after the adsorption of arsenate ions are illustrated in Figure 1. The mineral matter of the original AS material was rich in Ca and K phases, mainly as calcite and arcanite, respectively. P was incorporated in hydroxylapatite, whereas niter, quartz, kalsilite and magnesioferrite were detected in low amounts.

After biochar was modified by MgO, Figure 1b shows that periclase was formed on its surface. Following arsenate adsorption, a new crystalline phase was identified in the spectra of Figure 1c, sainfeldite (Ca<sub>5</sub>(AsO<sub>4</sub>)<sub>2</sub>(AsO<sub>3</sub>OH)<sub>2</sub>·4H<sub>2</sub>O), indicating that under alkaline conditions, As<sup>5+</sup> was removed by precipitation. To our knowledge, this mineral phase has not been reported previously for the adsorption of arsenate. The XRD of AS biochar modified by ZnO is represented in Figure 1d. Apart from the minerals detected for the raw material, zincite (ZnO) was identified after modification. Following arsenate adsorption, from Figure 1e, it can be seen that a new mineral phase claudetite (As<sub>2</sub>O<sub>3</sub>) was formed. This mineral was also detected in the XRD spectra of biochar modified by quarry dust after the adsorption of As<sup>5+</sup> (Figure 1g). Figure 1f,g also show the CaO of quarry dust after the adsorption of As<sup>5+</sup> (Figure 1g). Figure 1f,g also show that the CaO of quarry dust was transformed to portlandite (Ca(OH)<sub>2</sub>) after the activation of the biochar with steam. There is very limited information from the literature data on XRD results after arsenate adsorption by biochar materials. As<sup>5+</sup> precipitation was evidenced only in two reports, for calcium oxide-rich rice husk biochar [12] and dolomite-modified material [19].

The chemical functional groups on modified AS biochar, as detected by the FTIR, are indicated in Figure 2 and Table 2. In the case of Mg-modified material, the low-frequency peaks at wave numbers 434 cm<sup>-1</sup> and 538 cm<sup>-1</sup> are characteristic of the Mg-O composite [13,20]. The broad bands, shown in Figure 2a, at 1268 cm<sup>-1</sup> and 1580 cm<sup>-1</sup> are attributed to the C-O stretching vibration of alkyl/aryl ethers or aromatic esters and cycloalkenes, respectively. After As<sup>5+</sup> adsorption, the FTIR spectrum presented in Figure 2b was quite different. Strong intensities at 434 cm<sup>-1</sup> and 538 cm<sup>-1</sup> wave numbers disappeared, indicating that new bonding occurred between the Mg-O and As<sup>5+</sup> ion. Also, the new peaks, which appeared at wave numbers 640–1050 cm<sup>-1</sup>, represent the stretching vibration of As-O or As-OH bonds [4,7], confirming the adsorption of As<sup>5+</sup> on the biochar's surface. On the other hand, the disappearance of the 1268 cm<sup>-1</sup> peak after arsenate adsorption implies some interaction between C-O groups with As<sup>5+</sup> [1]. The new strong peak at 1442 cm<sup>-1</sup> and the weak one at 2372 cm<sup>-1</sup> are attributed to the C-H stretching of alkanes and the vibrational stretching of O=C=O, respectively. Furthermore, the new intense band at 3448 cm<sup>-1</sup>, shown in Figure 2b, which is attributed to hydroxyl group O-H vibrations, suggests that the O-H of water molecules were also adsorbed on the biochar's surface during the process [4].

When ASB was modified by ZnO/Zn(OH)<sub>2</sub>, Figure 2c shows that the introduction of this inorganic substance resulted in quite strong adsorption peaks between 450 cm<sup>-1</sup> and 950 cm<sup>-1</sup>, assigned to Zn-O vibrations [13] or bending vibrations of the hydroxyl groups in Zn-OH [3]. By comparing Figure 2c,d, corresponding to the Zn-modified spectra of the biochar before and after arsenate adsorption, it can be observed that several peaks are common in these graphs. Thus, the peaks at wave numbers 1384 cm<sup>-1</sup>, 1594/1642 cm<sup>-1</sup>, 2368 cm<sup>-1</sup> and 3494 cm<sup>-1</sup> are linked with stretching vibrations of O-H from alcohols/phenols, C=C from cycloalkenes and O=C=O and O-H from alcohol groups,

respectively.  $\text{As}^{5+}$  adsorption (Figure 2d) is indicated by the characteristic bands centered at  $652\text{ cm}^{-1}$  and  $884\text{ cm}^{-1}$ , representing As-O or As-OH bonds [4,7].

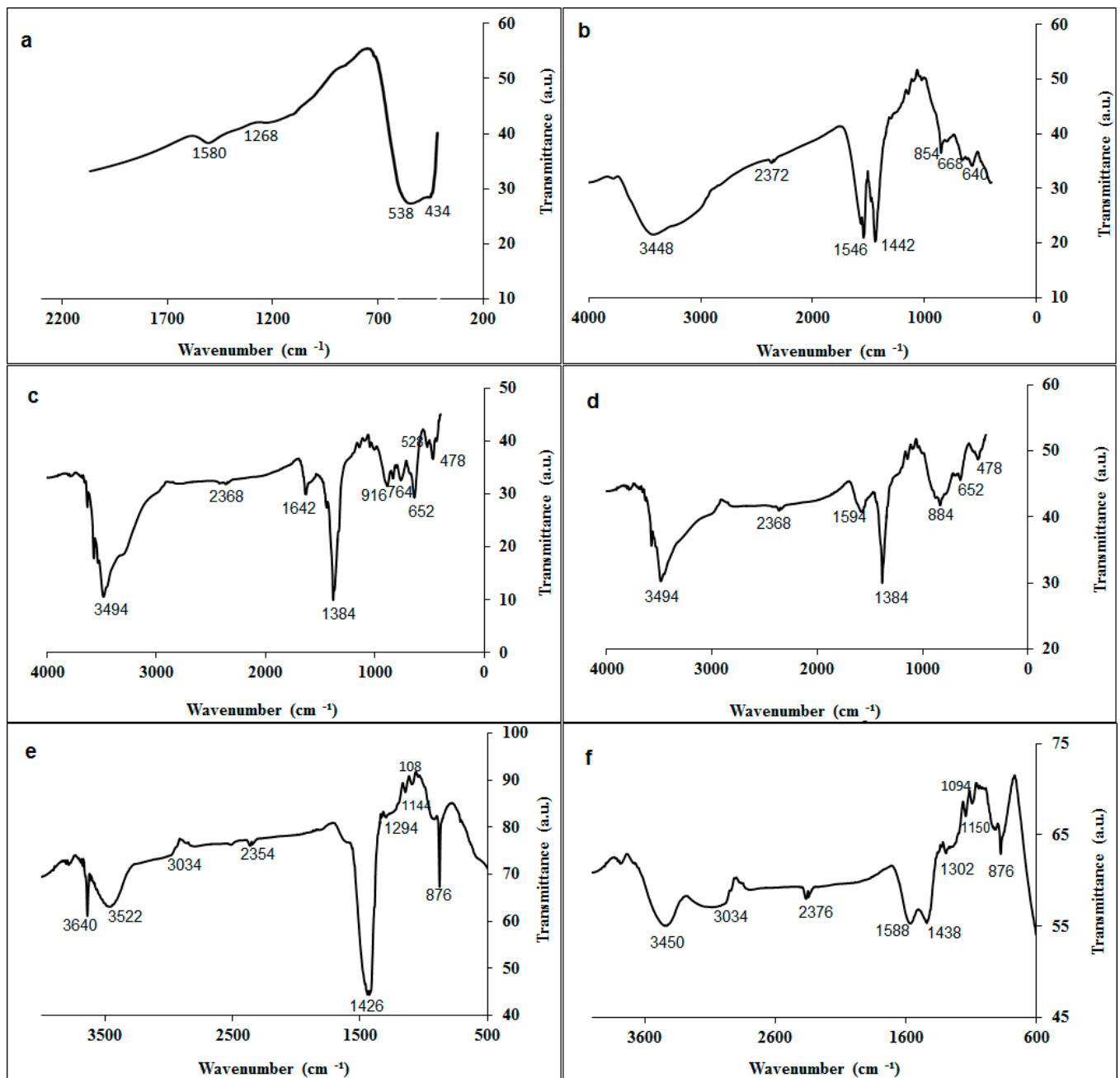


**Figure 2.** FTIR spectra of biochar modified by (a)  $\text{Mg}^{2+}$  prior to adsorption, (b)  $\text{Mg}^{2+}$  after adsorption, (c)  $\text{Zn}^{2+}$  prior to adsorption, (d)  $\text{Zn}^{2+}$  after adsorption, (e)  $\text{Ca}^{2+}$  prior to adsorption and (f)  $\text{Ca}^{2+}$  after adsorption.

The FTIR of ASB modified by quarry dust is illustrated in Figure 2e,f. At the  $876\text{ cm}^{-1}$  wave number, a strong vibration characteristic of Ca-O groups [21] of calcined quarry dust was shown in Figure 2e. Several small peaks in the region of  $1084\text{--}1294\text{ cm}^{-1}$  are attributed to the C-O stretching of alcohols, aliphatic ethers and aromatic esters. The intense absorbance band at  $1426\text{ cm}^{-1}$  represents the O-H bending of carboxylic acid, while the small peak at  $2354\text{ cm}^{-1}$  corresponds to the vibrational stretching of  $\text{O}=\text{C}=\text{O}$ . Broad bands between  $3034\text{ cm}^{-1}$  and  $3640\text{ cm}^{-1}$  are all representative of O-H groups from alcohols. After arsenate adsorption, from Figure 2f, it can be noticed that the intensity of the peak

corresponding to Ca-O bonds was considerably decreased, revealing some interaction of quarry dust with  $\text{As}^{5+}$  and possibly the overlapping of As-O, As-OH bonds in this region. Also, the peaks appearing in the 1084–1426  $\text{cm}^{-1}$  domain before adsorption were shifted to higher wave numbers after  $\text{As}^{5+}$  adsorption, 1094–1438  $\text{cm}^{-1}$ , implying  $\pi$ - $\pi$  interaction between the biochar matrix and  $\text{As}^{5+}$  [22]. The new broad band at 1588  $\text{cm}^{-1}$ , in Figure 2f, is assigned to cycloalkenes. All peaks at higher wave numbers (above 2000  $\text{cm}^{-1}$ ) found on quarry dust-modified material (Figure 2e), representing O=C=O and O-H stretching from alcohol groups, were also present after the adsorption of arsenate (Figure 2f).

**Table 2.** Chemical functional groups of modified biochar.

Modified Biochar	Wave Number ( $\text{cm}^{-1}$ )	Functional Groups
ASB-Mg	434/538	Mg-O
	640/668/854	As-O/As-OH
	1268	C-O
	1442	C-H
	1546/1580	C=C
	2372	O=C=O
	3448	O-H
ASB-Zn	478/528/652/764/884/916	Zn-O/Zn-OH
	652/884	As-O/As-OH
	1384	O-H
	1594/1642	C=C
	2368	O=C=O
	3494	O-H
ASB-Ca	876	Ca-O/As-O/As-OH
	1084/1144/1150/1294/1302	C-O
	1426/1438	O-H
	1588	C=C
	2354/2376	O=C=O
	3034/3450/3522/3640	O-H

### 3.2. Kinetics of Arsenate Adsorption

The effect of the contact time on the uptake of  $\text{As}^{5+}$  ions by ASB from the aqueous solution was studied within a time range of 0.5–24 h for an initial arsenate concentration of 10 mg/L. Figure 3 shows that arsenate delayed to adhere on the biochar surface and the adsorption rate was low, removing about 12% of arsenate from the solution in 3 h and 27% in 6 h. Then, it gradually decreased, finally achieving equilibrium in 12 h. The maximum removal of arsenate ions was 29.4% for an initial pH = 7 (at pH = 6, the efficiency was lower, so pH = 7 was selected for subsequent tests). This behavior implies a low bonding energy between the adsorbate and adsorbent, resulting in higher contact times, and this has also been observed in previous studies [8,11].

Two classical dynamic models (Equations (1) and (2)) were employed for the experimental data, and the characteristic parameters are displayed in Table 3. As can be seen, the model that was found to describe the experimental results more accurately was the pseudo-second-order model. According to this model, the reaction rate is proportional to the number of active sites on the surface of the adsorbent, and the rate-limiting step is chemisorption reaction. These findings greatly agree with the literature data [3,5,8,11,13,14].



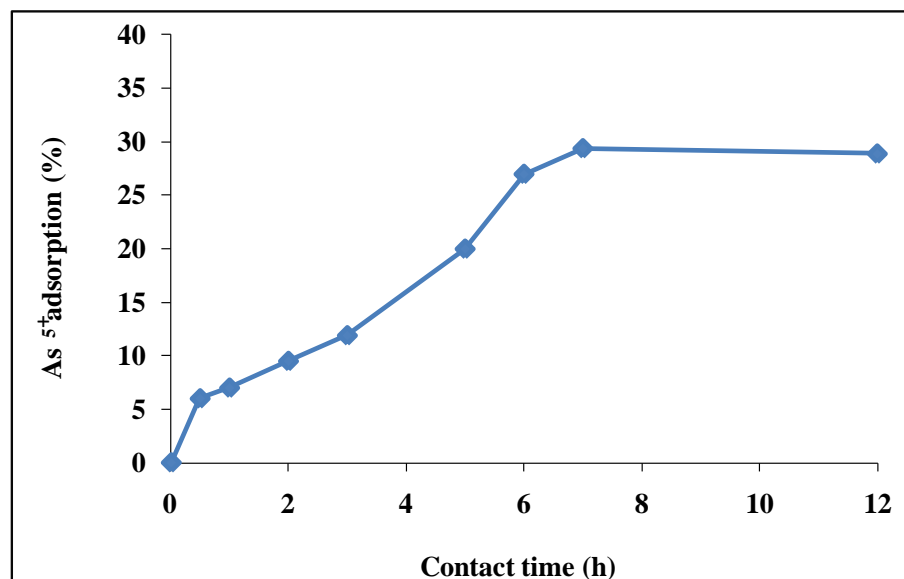


Figure 3. Kinetics of arsenate adsorption.

Table 3. Kinetic results of arsenate adsorption by ASB.

Kinetic Model Parameters					
Pseudo-First-Order			Pseudo-Second-Order		
q <sub>e</sub> (mg/g)	k <sub>1</sub> (1/h)	R <sup>2</sup>	q <sub>e</sub> (mg/g)	k <sub>2</sub> (1/h)	R <sup>2</sup>
0.733	0.009	0.427	0.733	0.973	0.759

### 3.3. Arsenate Adsorption Capacity of AS Biochar

The adsorption capacity of AS biochar, at various initial As<sup>5+</sup> concentrations in the solution and adsorbent dose, is compared with that of Mg-, Zn- and Ca-modified biochar in Table 4. As can be seen, at an adsorbent dose of 4 mg/L, the non-modified material showed a poor adsorption capacity for As<sup>5+</sup>, especially at low initial concentrations. The removal efficiency of As<sup>5+</sup> increased gradually with an increasing ion flux density, attaining a maximum of 49.4% at 100 mg/L As<sup>5+</sup>. This trend of favoring access to biochar's adsorption sites with a higher As<sup>5+</sup> concentration gradient, was also observed when the material was modified by quarry dust. However, the removal rate significantly increased in this case, and the maximum value was 97% at 100 mg/L As<sup>5+</sup>. For Mg- and Zn-modified biochar, it can be noticed that at low ion concentrations, up to 10 mg/L, arsenate was practically completely adsorbed by the solid, with the uptake rate declining thereafter at higher concentrations. For Mg-modified material, the removal efficiency was 86% at 100 mg/L As<sup>5+</sup>, while Zn-modified biochar presented an excellent performance for both low and high As<sup>5+</sup> concentrations, achieving the lowest value of 97% at 100 mg/L.

The effect of the adsorbent dosage plays a significant role in the removal efficiency of heavy metals from aqueous solutions. Table 4 shows that when the amount of biochar was lowered to 2 g/L, the adsorption of arsenate was improved (with the exception of Mg-modified material), agreeing with earlier studies [1,13].

Another critical parameter of the process, governing the surface charge of the biochar and the ionization of arsenate in the solution, is the pH. As arsenic is an anionic heavy metal, electrostatic attraction between the ion and the adsorbent would be favored under acidic conditions and weakened under alkaline conditions. At a basic pH, As<sup>5+</sup> species exist as HAsO<sub>4</sub><sup>2-</sup> [7,13,14]. From Table 4, presenting the solution pH before and after As<sup>5+</sup> adsorption at equilibrium, it can be observed that the pH was alkaline throughout the process and the adsorption efficiency increased with the pH, reaching maximum values at pH values between 9.7 and 11.5. As AS biochar was found to be alkaline (pH = 10.2)

and abundant in negatively charged functional groups (identified by FTIR), this implies that As<sup>5+</sup> ions interacted with –O-H groups on the solid surface through ligand exchange, releasing them into the solution. Some previous studies [3,14] also reported that adsorption between negatively charged oxyanions of As<sup>5+</sup> and ZnO might occur through the ligand exchange of the hydroxyl group from Zn-OH, as the removal percentage of As<sup>5+</sup> was enhanced with increasing pH values. Furthermore, others reported that for Mg- or Ca-modified materials, MgO [17,20] or CaO [12] were positively charged on the biochar’s surface, efficiently removing As<sup>5+</sup> ions from alkaline solutions. Possible mechanisms for the current results will be discussed below.

**Table 4.** Removal efficiency of arsenate for various initial concentrations and adsorbent doses.

Initial Ion Concentration (mg/L)	Adsorbent Dose 4 g/L							
	Removal Efficiency (%)				pH after Adsorption			
	ASB	ASB-Mg	ASB-Zn	ASB-Ca	ASB	ASB-Mg	ASB-Zn	ASB-Ca
5	2.2	99.9	100.0	89.0	8.02	9.97	9.58	11.19
10	29.3	99.1	100.0	94.0	7.89	9.65	9.34	11.85
25	24.4	96.0	98.5	95.8	7.90	9.60	9.17	11.77
50	41.2	77.0	98.4	96.2	7.96	9.56	8.90	11.63
75	45.2	85.0	98.0	96.7	7.99	9.46	8.78	11.58
100	49.4	86.0	97.0	97.0	8.04	9.33	8.71	11.48
Adsorbent Dose 2 g/L								
5	2.9	94.0	100.0	92.0	7.90	10.05	9.65	11.2
10	30.0	93.3	100.0	95.0	7.81	9.81	9.32	11.9
25	31.2	82.2	99.7	97.0	7.83	9.75	9.15	11.8
50	45.1	64.3	98.8	97.3	7.88	9.65	8.92	11.6
75	46.9	63.8	99.1	97.7	7.91	9.55	8.87	11.6
100	50.6	62.7	99.9	98.0	7.97	9.47	8.80	11.5

### 3.4. Equilibrium of Arsenate Adsorption

The arsenate uptake of the ASB adsorbent was simulated by the Langmuir and Freundlich models. The adsorption isotherms, which were defined in the experimental section at equilibrium conditions, are illustrated in Figures 4–7, and calculated parameters are included in Table 5. All arsenate equilibrium test data were best fitted with the Freundlich model, conforming the theory that arsenate molecules migrated to heterogeneous surface sites on the biochar, following a multilayer adsorption mechanism, instead of a monolayer mechanism assumed by the Langmuir model. The Freundlich correlation coefficient ranged between 0.94 and 0.97, as opposed to the Langmuir correlation coefficient, which varied between 0.42 and 0.83 for the biochar-modified material.

**Table 5.** Model results of arsenate adsorption by non-modified or modified ASB.

	Adsorbent Dose 4 g/L					
	Langmuir Model			Freundlich Model		
	Q (mg/g)	b (L/mg)	R <sup>2</sup>	k (L/g)	1/n	R <sup>2</sup>
ASB	12.469	0.009	0.205	0.126	1.080	0.888
ASB-Mg	15.528	0.945	0.773	6.092	0.331	0.941
ASB-Zn	26.666	1.974	0.835	12.981	0.325	0.943
ASB-Ca	20.533	0.188	0.819	5.375	1.325	0.993
Adsorbent Dose 2 g/L						
ASB	81.301	0.585	0.508	27.327	0.698	0.810
ASB-Mg	33.333	0.126	0.838	4.795	0.487	0.977
ASB-Zn	39.062	9.143	0.714	66.512	0.637	0.889
ASB-Ca	16.0	0.416	0.602	15.170	1.800	0.973

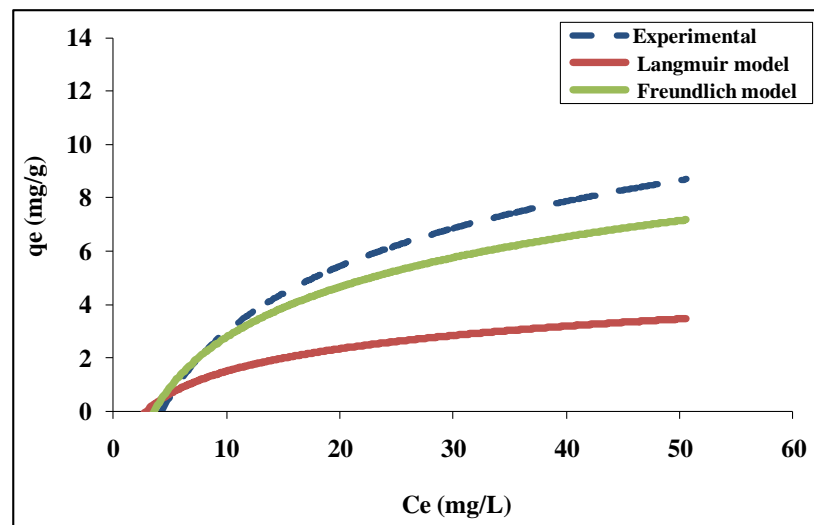


Figure 4. Isotherms of the original biochar at an adsorption dose of 4 g/L.

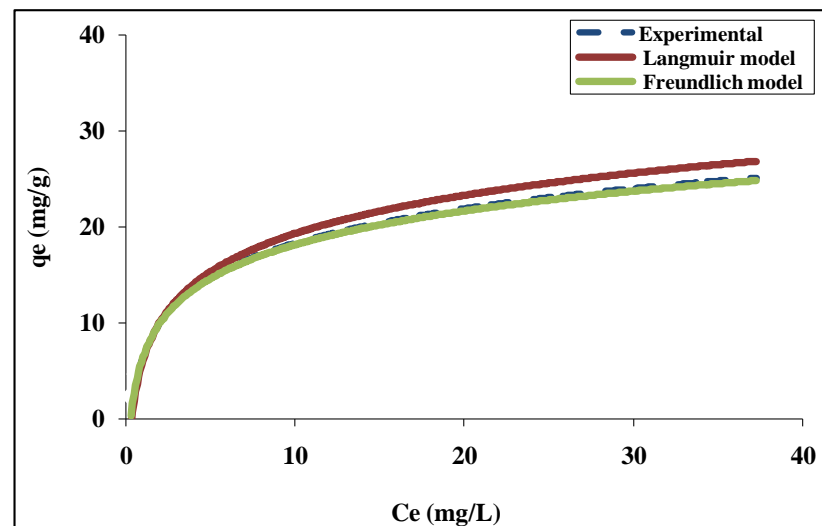


Figure 5. Isotherms of the Mg-modified biochar at an adsorption dose of 2 g/L.

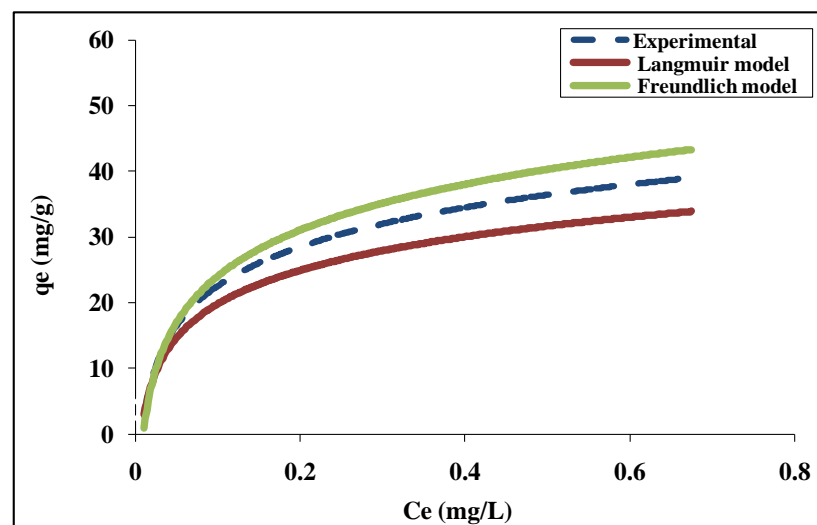
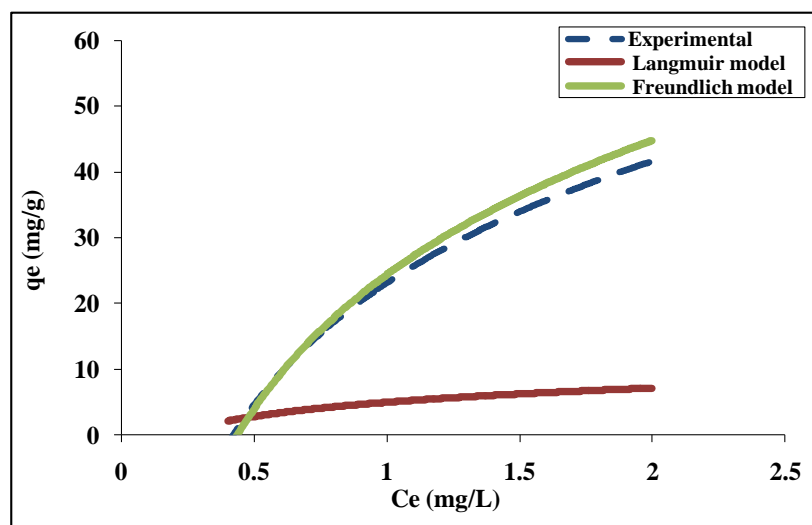


Figure 6. Isotherms of the Zn-modified biochar at an adsorption dose of 2 g/L.



**Figure 7.** Isotherms of the Ca-modified biochar at an adsorption dose of 2 g/L.

Past investigations using a variety of materials and modifiers reported that either the Freundlich [3,12,13] or Langmuir [4,5,7,10,14] models best described the equilibrium  $\text{As}^{5+}$  concentration and sorption capacity, pointing to the complexity of the adsorption mechanism. The present results showed that for non-modified ASB, the maximum adsorption capacity was 12.4 mg/g, which is higher than the values determined (0.8–7.1 mg/g) for similar materials [1,7,8,11,14]. However, for modified material by Mg, Zn or Ca oxides, the maximum value was increased to 21.5 mg/g, 24.3 mg/g and 24.3 mg/g, respectively. On the other hand, the maximum capacity of ASB for  $\text{As}^{5+}$  adsorption could be enhanced up to 35 mg/g, 50 mg/g and 49 mg/g for Mg-, Zn- and Ca -modified material, respectively, in case the adsorbent dose is 2 g/L (Figures 5–7). Previous studies for MnO-modified corn straw biochar reported a maximum adsorption capacity for  $\text{As}^{5+}$  of 14.4 mg/g [1]; for KOH-modified municipal solid wastes, a value of 31 mg/g was reported [11]; and for ZnO-modified corn cobs, a value of 25.9 mg/g was reported [14]. On the other hand, for Fe-coated biochars of rice husks, walnut shells, cotton wood and pine sawdust, the maximum  $\text{As}^{5+}$  capacities were found to range between 0.1 mg/g and 43.7 mg/g [5–7,10,12]. A comparison with the current results is made in Table 6.

**Table 6.** Comparison of the literature data with the current results.

Feedstock	Activation Method	Adsorbent Dose (g/L)	Arsenate Adsorption Capacity (mg/g)	Reference
Empty fruit bunch			5.5	
Rice husk	Commercial biochar	5	7.1	[7]
Fe-coated rice husk			16	
Roots of <i>C. esculenta</i>	Nitrogen/steam 700 °C	0.6	2.2	[8]
Corn cob	Nitrogen 600 °C	4	5	[14]
ZnO-corn cob			25.9	
MnO-corn straw	Nitrogen 600 °C	0.5–4	14.4	[1]
KOH-MSW	Nitrogen 600 °C	2	31	[11]
Fe-coated walnut shell	Nitrogen microwave	1	1.9	[5]
Fe-coated pine sawdust	Nitrogen 600 °C	0.2	43.7	[6]
Fe-coated cotton wood	Nitrogen 600 °C	2	3.1	[10]
Fe-coated rice husk	Nitrogen 300 °C	16	0.7	[12]
Almond shell			12.4	
Mg/Zn/Ca-almond shell	Nitrogen/steam 700 °C	2	35/50/49	This study

### 3.5. Mechanisms of Arsenate Adsorption

An improved adsorption of  $\text{As}^{5+}$  on biochar can be achieved by enlarging its surface area and optimizing its porosity. However, this is not the only criterion for the efficient removal of  $\text{As}^{5+}$  and does not always increase the adsorption capacity [9,11,12]. Other mechanisms also play important roles such as electrostatic attraction, anion exchange, chemical complexation, electron coordination, and surface precipitation [2,3,7,11–14].

As previously presented by the ultimate analysis and the FTIR spectra, the biochar under study was enriched in oxygen and incorporated in negatively charged functional groups. Also, it was shown that the pH was alkaline throughout the adsorption process and  $\text{As}^{5+}$  species existed as  $\text{HAsO}_4^{2-}$  in the solution. Furthermore, for all modified materials, it was shown that the adsorption efficiency increased with the pH, reaching maximum values at pH = 9.7–11.5. Therefore, the ligand exchange between  $\text{As}^{5+}$  ions and hydroxyl groups from Ca-OH, Mg-OH or Zn-OH on a solid surface appeared to be the mechanism of  $\text{As}^{5+}$  adsorption, while electrostatic attraction was not possible. These findings are supported by previous studies [3,8,14].

The type and concentration of biochar's surface functional groups are known to significantly control the adsorption capacity of organic or inorganic sorbents [7,11,13]. Through FTIR analysis, it was shown that, after arsenate adsorption As-O and As-OH bonds appeared on biochar's surface for all modified materials. Moreover, the decrease in Ca-O and the disappearance of Mg-O peaks after adsorption imply some interaction of quarry dust and MgO with  $\text{As}^{5+}$ , respectively. Consequently, another mechanism responsible for the adsorption of  $\text{As}^{5+}$  could be chemical complexation between  $\text{As}^{5+}$  and the functional groups of the adsorbent. Also, for quarry dust-modified biochar, the shifting of peaks to higher wave numbers after adsorption reveals electron coordination between the  $\text{As}^{5+}$  ion and adsorbent matrix as a potential adsorption mechanism. These results are in agreement with the majority of previous investigations reporting such mechanisms [4,7,9,11,13,22].

Furthermore, according to the XRD spectra presented above and analyzed, arsenate was found to be removed from the solution by precipitation with inorganic or organic species of biochar, as new mineral phases were detected after adsorption from MgO-, ZnO- and CaO-modified material, sainfeldite and claudetite, respectively. Therefore, surface precipitation was also identified as an important  $\text{As}^{5+}$  adsorption mechanism, in agreement with some other studies [12,17]. The sorption mechanisms are shown in Figure 8.

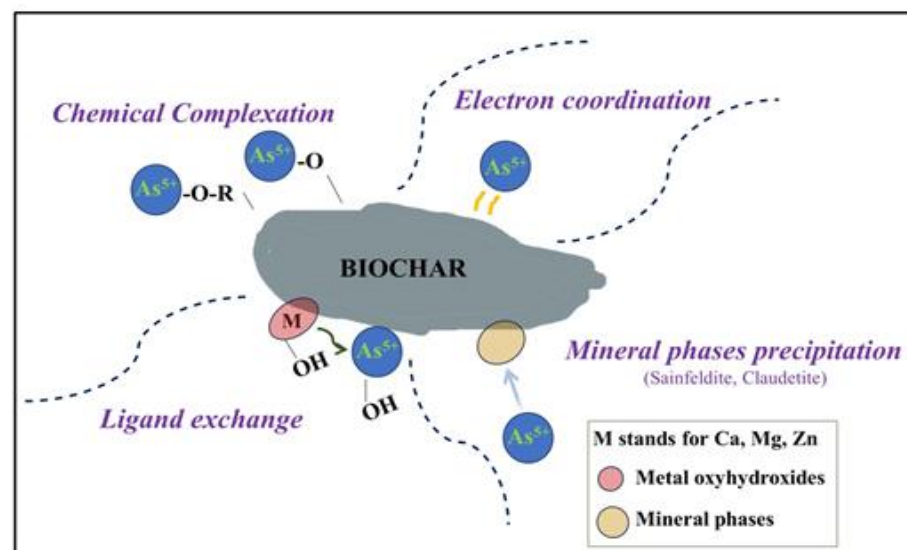


Figure 8. Mechanisms of arsenate sorption.



#### 4. Conclusions

Almond shell biochar presented a negatively charged surface. The adsorption of arsenate occurred by chemisorption and attained equilibrium in 12 h, with a maximum removal efficiency of 29.4%, at an initial concentration of 10 mg/L. The modification of biochar by Mg, Zn or Ca oxides increased the removal rate significantly, from 49.4% at 100 mg/L As<sup>5+</sup> up to 86%, 97% and 97%, respectively. Zn-modified biochar presented an excellent performance for both low and high As<sup>5+</sup> concentrations.

All experimental data were accurately fitted by the Freundlich isotherm model ( $R^2 = 0.94\text{--}0.97$ ), indicating a multilayer adsorption mechanism. When the adsorbent dose was 4 g/L, the arsenate adsorption capacity of biochar increased after Mg-, Zn- or Ca-modification from 12.4 mg/g to 21.5 mg/g, 24.3 mg/g and 24.3 mg/g, respectively. For an adsorbent dose of 2 g/L, these values were raised up to 35 mg/g, 50 mg/g and 49 mg/g, respectively.

Structural analyses, pH measurements, X-ray diffraction and Fourier Transform Infrared analyses, before and after the adsorption of the As<sup>5+</sup> ion, showed that ligand exchange between As<sup>5+</sup> ions and hydroxyl groups on the biochar's surface, chemical complexation between the As<sup>5+</sup> ion and the adsorbent as well as surface precipitation with modified biochar species were the potential mechanisms of adsorption. For quarry dust-modified material, electron coordination was also a possible mechanism.

**Author Contributions:** Conceptualization, D.V.; methodology, D.V. and D.P.; software, E.S. and A.S.; validation, D.V. and D.P.; investigation, D.V. and D.P.; data curation, D.P., E.S. and A.S.; writing—original draft preparation, D.V.; writing—review and editing, D.V.; visualization, D.V.; supervision, D.V. All authors have read and agreed to the published version of the manuscript.

**Funding:** This research received no external funding.

**Data Availability Statement:** The original contributions presented in the study are included in the article, further inquiries can be directed to the corresponding author/s.

**Acknowledgments:** The authors kindly thank the laboratories of Hydrocarbons Chemistry and Ore Processing and Beneficiation of the Technical University of Crete for the ultimate and FTIR analysis and T. Ioannides and M. Smyrnioti from the Inst. of Chemical Engineering Sciences in Patra for the BET measurements of the samples.

**Conflicts of Interest:** The authors declare no conflicts of interest.

#### References

1. Yu, Z.; Zhou, L.; Huang, Y.; Song, Z.; Qiu, W. Effects of a manganese-oxide-modified biochar composite on adsorption of arsenic in red soil. *J. Environ. Manag.* **2015**, *163*, 155–162. [[CrossRef](#)] [[PubMed](#)]
2. Braghiroli, F.L.; Calugaru, I.L.; Merchan, C.G.; Neculita, C.M.; Bouafif, H.; Koubaa, A. Efficiency of eight modified materials for As (V) removal from synthetic and real mine effluents. *Miner. Eng.* **2020**, *151*, 106310. [[CrossRef](#)]
3. Xia, D.; Tan, F.; Zhang, C.; Jiang, X.; Chen, Z.; Li, H.; Zheng, Y.; Li, Q.; Wang, Y. ZnCl<sub>2</sub>-activated biochar from biogas residue facilitates aqueous As (III) removal. *Appl. Surf. Sci.* **2016**, *377*, 361–369. [[CrossRef](#)]
4. Zhu, N.; Yan, T.; Qiao, J.; Cao, H. Adsorption of arsenic, phosphorous and chromium by bismuth impregnated biochar: Adsorption mechanism and depleted adsorbent utilization. *Chemosphere* **2016**, *164*, 32–40. [[CrossRef](#)] [[PubMed](#)]
5. Duan, X.; Zhang, C.; Srinivasakannan, C.; Wang, X. Waste walnut shell valorization to iron loaded biochar and its application to arsenic removal. *Res. Effic. Technol.* **2017**, *3*, 29–36.
6. Liu, Z.; Zhang, F.; Sasai, R. Arsenate removal from water using Fe<sub>3</sub>O<sub>4</sub>-loaded activated carbon prepared from waste biomass. *Chem. Eng. J.* **2010**, *160*, 57–62. [[CrossRef](#)]
7. Samsuri, A.W.; Zadeh, F.S.; Bardan, B.J.S. Adsorption of As (III) and As (V) by Fe coated biochars and biochars produced from empty fruit bunch and rice husk. *J. Environ. Chem. Eng.* **2013**, *1*, 981–988. [[CrossRef](#)]
8. Banerjee, S.; Mukherjee, S.; LaminKa-Ot, A.; Joshi, S.R.; Mandal, T.; Halder, G. Biosorptive uptake of Fe<sup>2+</sup>, Cu<sup>2+</sup> and As<sup>5+</sup> by activated biochar derived from *Colocasia esculenta*: Isotherm, kinetics, thermodynamics and cost estimation. *J. Adv. Res.* **2016**, *7*, 597–610. [[CrossRef](#)]
9. Alatalo, S.; Repo, E.; Makila, E.; Salonen, J.; Vakkilainen, E.; Sillanpaa, M. Adsorption behaviour of hydrothermally treated municipal sludge and pulp and paper industry sludge. *Biores. Technol.* **2013**, *147*, 71–76. [[CrossRef](#)]
10. Zhang, M.; Gao, B.; Varnoosfaderani, S.; Hebard, A.; Yao, Y.; Inyang, M. Preparation and characterization of a novel magnetic biochar for arsenic removal. *Biores. Technol.* **2013**, *130*, 457–462. [[CrossRef](#)]

11. Jin, H.; Capareda, S.; Chang, Z.; Gao, J.; Xu, Y.; Zhang, J. Biochar pyrolytically produced from municipal solid wastes for aqueous As (V) removal: Adsorption property and its improvement with KOH. *Biores. Technol.* **2014**, *169*, 622–629. [[CrossRef](#)] [[PubMed](#)]
12. Agrafioti, E.; Kalderis, D.; Diamadopoulos, E.J. Ca and Fe modified biochars as adsorbents of arsenic and chromium in aqueous solutions. *Environ. Manag.* **2014**, *146*, 444–450. [[CrossRef](#)] [[PubMed](#)]
13. Li, Q.; Liang, W.; Liu, F.; Wang, G.; Wan, J.; Zhang, W.; Peng, C.; Yang, J. Simultaneous immobilization of arsenic, lead and cadmium by magnesium-aluminum modified biochar in mining soil. *J. Environ. Manag.* **2022**, *310*, 114792. [[CrossRef](#)] [[PubMed](#)]
14. Cruz, G.J.F.; Mondal, D.; Rimaycuna, J.; Soukup, K.; Gomez, M.M.; Solis, J.L.; Lang, J. Agrowaste derived biochars impregnated with ZnO for removal of arsenic and lead in water. *J. Environ. Chem. Eng.* **2020**, *8*, 103800. [[CrossRef](#)]
15. Chen, M.; Bao, C.; Hu, D.; Jin, X.; Huang, Q. Facile and low-cost fabrication of ZnO/biochar nanocomposites from jute fibers for efficient and stable photodegradation of methylene blue dye. *J. Anal. Appl. Pyrolysis* **2019**, *139*, 319–332. [[CrossRef](#)]
16. Vamvuka, D.; Elmazaj, J.; Berkis, M. Enhanced H<sub>2</sub> gas production from steam gasification of a winery waste through CO<sub>2</sub> capture by waste concrete fines and use of alkali catalysts. *Renew. Energy* **2023**, *219*, 119428. [[CrossRef](#)]
17. Jiang, M.; Yang, Y.; Lei, T.; Ye, Z.; Huang, S.; Fu, X.; Liu, P.; Li, H. Removal of phosphate by a novel activated sewage sludge biochar: Equilibrium, kinetic and mechanism studies. *Appl. Ener. Comb. Sci.* **2022**, *9*, 100056. [[CrossRef](#)]
18. Hassan, M.; Liu, Y.; Naidu, R.; Parikh, S.J.; Du, J.; Qi, F.; Willett, I.R. Influences of feedstock sources and pyrolysis temperature on the properties of biochar and functionality as adsorbents: A meta-analysis. *Sci. Tot. Environ.* **2020**, *744*, 140714. [[CrossRef](#)]
19. Salameh, Y.; Albadarin, A.B.; Allen, S.; Walker, G.; Ahmad, M.N.M. Arsenic (III, V) adsorption onto charred dolomite: Charring optimization and batch studies. *Chem. Eng. J.* **2015**, *259*, 663–671. [[CrossRef](#)]
20. Shin, H.; Tiwari, D.; Kim, D.J. Phosphate adsorption/desorption kinetics and P bioavailability of Mg-biochar from ground coffee waste. *J. Water Process Eng.* **2020**, *37*, 101484. [[CrossRef](#)]
21. Li, J.; Li, B.; Huang, H.; Lv, X.; Zhao, N.; Guo, G.; Zhang, D. Removal of phosphate from aqueous solution by dolomite-modified biochar derived from urban dewatered sewage sludge. *Sci. Tot. Environ.* **2019**, *687*, 460–469. [[CrossRef](#)] [[PubMed](#)]
22. Li, R.; Wang, J.J.; Zhou, B.; Zhang, Z.; Liu, S.; Lei, S.; Xiao, R. Simultaneous capture removal of phosphate, ammonium and organic substances by MgO impregnated biochar and its potential use in swine wastewater treatment. *J. Clean. Prod.* **2017**, *147*, 96–107. [[CrossRef](#)]

**Disclaimer/Publisher’s Note:** The statements, opinions and data contained in all publications are solely those of the individual author(s) and contributor(s) and not of MDPI and/or the editor(s). MDPI and/or the editor(s) disclaim responsibility for any injury to people or property resulting from any ideas, methods, instructions or products referred to in the content.